Transmission of 10 Gbps C-band-signal-based Radio Over Fiber for Next Generation Communication Systems

Hasan k. Al Deen[1] and Haider J. Abd[1,2]

[1]*University of Babylon, Babylon, Iraq,*
[2]*Al-Mustaqbal University, Hilla, Iraq*

Abstract — Rapid development of 5G networks encourages researchers to improve the radio-over-fiber (RoF) technique in order to reach 10 Gbps data transmission rates, to increase bandwidth and range, while reducing latency and implementation cost. This paper evaluates an analog radio-over-fiber (ARoF) technique that is compatible with long-distance communication systems. We demonstrate a long distance transmission of a 28 GHz 64 QAM signal via a single mode fiber (SMF) after modulating it with the use of two parallel Mach-Zehnder modulators, without any optical amplifiers. The results show that our prototype solution is capable of transferring data over distances of up to 140 km, via SMF, with a 10 Gbps data rate. The error vector magnitude (EVM) was found to be 7.709%. The proposed system offers exceptional capabilities in terms of supporting high bitrates, while ensuring that EVM remains within the 3GPP limits. Compared to other works, the proposed solution proves to be superior in terms of performance, making it an ideal choice for next generation long-haul communication systems.

Keywords — 5G, 64 QAM, ARoF, C-RAN, EVM, mmWave

1. Introduction

Fifth generation (5G) telecommunication networks are considered to be the core of intelligent communication, as the offer smart connectivity, ensure quicker communication and enable holographic connectivity [1]. Radio-over-fiber-based centralized radio access networks (C-RAN) can be a powerful tool for reducing operating costs and shifting the overall expense-related burden from user equipment (UE) to base station (BS). With the help of this particular technique, signals may be sent over vast distances and through heavily crowded locations. Large-scale opportunities exist in this field for basic and applied research and development, focusing on boosting bitrates and lowering impairment impacts [2].

Due to the growing demand and increasing network densities, the radio frequency (RF) spectrum available in high-frequency bands is teetering towards constant saturation. The high capacity of optical fiber solutions and flexibility of wireless access techniques may be combined effectively by relying on RoF systems which offer a good trade-off between data broadcast capacity, usability, as well as overall installation and maintenance expenses [3].

Millimeter wave (mmWave) systems are considered to be one of the likely spectrum options for 5G communications, due to their significant accessible bandwidth. 5G will require current spectrum and mmWave frequency bands to achieve high capacity. Large antenna arrays will be needed as well to help ease the difficult propagation conditions at frequencies ranging from 24 GHz to 30 GHz, 37 GHz to 40 GHz, and in the 52 GHz band [4].

Two types of RoF may be distinguished: ARoF (analog) and DRoF (digital). In the ARoF technique, the RF signal modulates on an optical carrier, with the benefit of great spectrum effectiveness. Such a technique is most frequently employed to modulate a data signal on an optical carrier. Although it encourages straightforward designs of distant radio devices, as a photodetector is all that is required to reconstruct the analog waveform, it is susceptible to non-linearities in used components used [5].

In the DRoF technique, the signal is sent through the fiber as a binary stream, making it resistant to non-linearity. However, because it requires the use of analog-to-digital converters in the distant radio unit, characterized by high power consumption at high sampling rates, DRoF is sometimes perceived as less appealing.

Figure 1 demonstrates a C-RAN-based ARoF mobile front haul design. At the control station (CS), RF signal is created by upconverting the baseband signal. The optical modulator is responsible for the next phase of the RoF system, as it converts the RF signal from electrical to optical form, before transmitting it through the optical fiber. Various modulation techniques may be employed in the CS to create a resilient signal when executing the modulation process, which acquires a higher signal quality at the following stage.
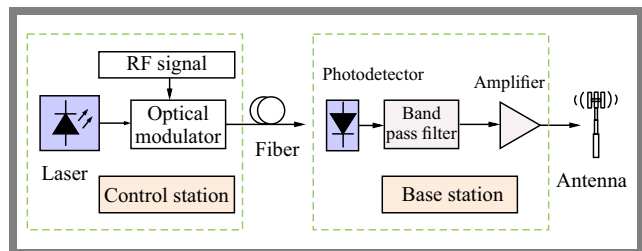

Fig. 1. General C-RAN-based ARoF scheme.

Next, at the base station, the photodetector diode (PD) converts the received optical signal back into tan electrical form. Then, the signal is filtered and amplified before being sent through the antenna. It needs to be born in mind, however, that the electrical and optical components used may introduce non-linearities into the signal's transmitting path [6]. A multi-mode fiber is a better choice for short-haul systems than the single-mode variety, with the latter being better suited for long-haul systems [7]. The bit error rate (BER) and quality factor (Q) obtained with the use of an avalanche photodiode (APD) diode are superior to those obtained while relying on a PIN photodiode [8].

2. Related Work

The high requirements of 5G force the researchers to use advanced modulation techniques with high-frequency bands to achieve high data rates, while maintaining simplicity and cost efficiency. Thus, there was a need to improve system performance and overcome non-linear impairments affecting ARoF links.

Several techniques have been introduced to improve the RoF architecture. In [9], the researchers analyze three optical modulation types: electro-absorption modulator (EAM), directly modulated laser (DML), Mach-Zehnder modulator (MZM) or external modulator. They provide an outdoor free-space RF channel of 50 m with 16 QAM, demonstrating that transmitters can operate under the EVM limit of 13.5%.

A 32 QAM signal directly modulated at 28 GHz on a vertical-cavity surface-emitting laser (VCSEL) is studied in [10]. The 2 km standard SMF transmission resulted in an EVM of 8.02%. It is advised to use a DML to transmit a 64 QAM 24 GHz signal over a RoF system in free space in article [11], while in [12], the researchers show that a straightforward 24 GHz RoF transmission system design is capable of supporting a Gbps-class data rate for various transmission spans in the construction of a RAN, and that 6 Gbps 64 QAM signals can be successfully spread after 20 and 50 km optical fiber and 1-meter wireless spread with EVM of 5.98% and 6.87%, respectively.

10-Msymbols/s QAM 16 externally modulated optical links for RoF applications were analyzed in the context of linearity of MZM and 16 QAM modulations over 20 km of SMF. The results show that the system is limited to less than 35 dBc (decibels relative to the carrier) in terms of adjacent channel leakage ratio (ACLR) and its BER $<10^{-3}$ [13]. A dual-drive Mach-Zehnder modulator (DDMZM) fed by baseband signals is tested for various transmission rates in article [14]. The QAM modulation technique improves spectral efficiency and results in faster-rate data transmissions in constrained frequency bands. A fiber-fronthaul link with a 2.5 Gbps 64 QAM signal for 4G LTE and 5G NR-oriented networks was established using an ARoF system [15]. The results showed compatibility with known calculations and experimental data, depending on transmission distance and economic requirements.

Undoubtedly, within the realm of upcoming long-haul communication systems, the paramount challenges lie in achieving high data rates, minimizing latency, and ensuring cost-efficiency. This paper serves as a compelling demonstration of these critical imperatives. We demonstrate a 10 Gbps transmission relying on ARoF technology that is suitable for modern C-band communication systems. The 64 QAM signal is transmitted through a 140 km section of SMF, with decent performance. With the use of the parallel MZM technique and dispersion compensating fiber (DCF), the length of the transmission link is increased. Then, the system's parameters, such as continuous wave (CW) laser power, MZMs extinction ratio, and phase shift angle, are examined to achieve the best EVM.

Section 3 describes the architecture of the proposed system, its key components, and the principle of analog RoF at high-frequency bands. The effectiveness of the model is demonstrated by comparing the presented model with earlier works. Section 4 analyzes and discusses the simulation results and the system's performance. Finally, conclusions are drawn in Section 5.

3. Key Components of the System

3.1. System Setup

The proposed ARoF system was designed and tested using Optisystem software, as illustrated in Fig. 2. At the transmitter, the original signal is generated with 64 QAM symbol mapping (encoded at 6 bits per symbol) and a bit stream produced by a pseudo-random binary sequence (PRBS). In the QAM modulator block, serial-to-parallel conversion is performed by utilizing a QAM signal generator which divides the stream into two parallel subsequences sent in two quadrature carriers. The subsequences are up-sampled for I and Q signals by digitally up-converting the resultant NRZ bit streams of the I and Q channels to a carrier frequency (f_c) of 28 GHz. Equation (1) describes the baseband I and Q signal [16]:

$$S(t) = I(t)\sin\omega_c t + Q(t)\cos\omega_c t , \qquad (1)$$

where ω_c is the angular frequency of the carrier signal.

Next, the electrical QAM signal is duplicated into two instances. The upper part undergoes a phase shift of –90° before being fed to MZM_1, while the lower part is shifted by 90° before being fed to MZM_2. Subsequently, an optical power combiner recombines the outputs from both MZMs, and the resulting signal is transmitted through the optical fiber to the BS.

3.2. Optical Signal

A 1550 nm CW laser and an E/O converter with the average output power of 10 dBm and a linewidth of 0.1 MHz are used in the optical link. The output electric field of the optical signal can be described as:
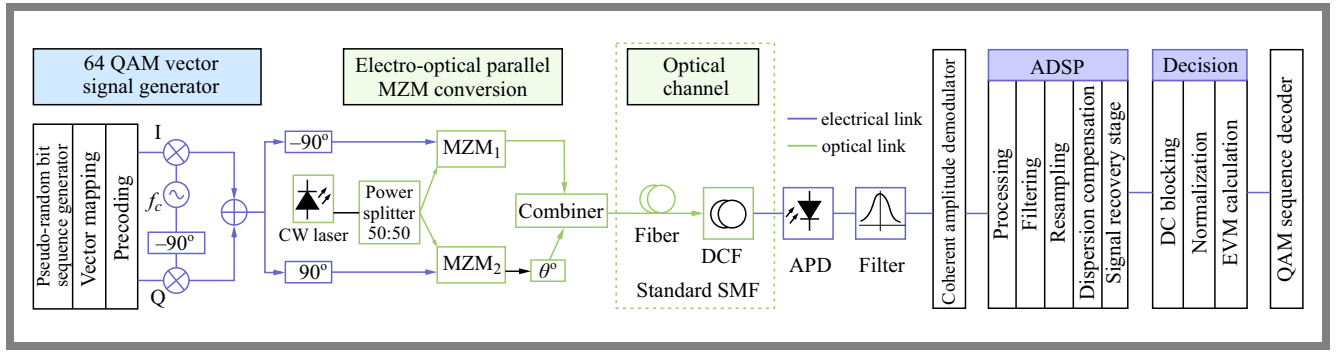
$$E_{cw}(t) = E_0\, e^{j\omega_0 t} , \qquad (2)$$

Fig. 2. Overall proposed system setup.

where E_0 is the amplitude and ω_0 is the angular frequency of the electric field [17].

The output of the CW laser is split into two equal beams using a power splitter with a splitting ratio of 50:50, before connecting to MZMs. A phase shifter of $\pi/2$ shifts this modulator output. Then, the MZMs output is combined using an optical combiner. Thus, two parallel MZMs modify the QAM signal with light waves produced by a laser. The MZM extinction ratio (ER) is optimized to ensure the system performance of the entire system. The equations describing the behaviors of the MZM that is an intensity modulator based on an interferometric principle are:

$$E_{out}(t) = E_{cw}(t) \cos \Delta\theta(t)\, e^{j\Delta\phi(t)}\,. \qquad (3)$$

$\Delta\theta(t)$ is the phase difference between the two branches of the MZM and is described as follows:

$$\theta(t) = \frac{\pi}{2}\Big[0.5 - ER\big(S(t) - 0.5\big)\Big]\,, \qquad (4)$$

where E_R is the extinction ratio, $S(t)$ is the input electrical signal normalized between 0 and 1, and $\Delta\phi(t)$ is the signal phase change, such that:

$$\Delta\phi(t) = \Delta\theta(t) \times \frac{1 + SF}{1 - SF}\,. \qquad (5)$$

SF is the symmetry factor which characterizes the asymmetry between the two arms of the MZM. When the MZM is perfectly symmetric, the voltages applied to both arms are equal, resulting in balanced phase modulation.

The structure can be modelled in the first approximation with the following linearized model (neglecting modulator chirp) [18]:

$$E_1(t) = \frac{E_{cw}(t)}{2} \cos \Delta\theta_1(t)\, e^{j\Delta\phi_1(t)}\,, \qquad (6)$$

$$E_2(t) = \frac{E_{cw}(t)}{2} \cos \Delta\theta_2(t)\, e^{j\Delta\phi_2(t)}\,, \qquad (7)$$

$$E_{out}(t) = \frac{E_{cw}(t)}{2}\big(E_1(t) + E_2(t)\big)\, e^{j\theta_0}\,, \qquad (8)$$

where θ_o is the phase angle that shifts the output of MZM$_2$ to get the best EVM result, in this work, it is found to be $(-\pi/2)$.

3.3. Optical Channels

A 140 km long SMF with an attenuation factor of 0.2 dB/km is used for carrying the optical signal to the BS. These signals exhibit chromatic dispersion (CD) being a major source of non-linearity phenomena affecting the analog signal. DCF provides an optical medium with a negative CD at the operating point to compensate the CD effect that occurred in SMF. A 140 km SMF with a CD of 17 ps/nm/km is characterized by the total cumulative dispersion of 17×140 = 2380 ps/nm. This value can be compensated by using a 28 km long DCF with a –85 ps/km/nm dispersion factor. Therefore, total compensated dispersion is 28×(–85)=–2380 ps/nm. This means that zero dispersion is achieved and full compensation is reached [19].

3.4. Base Station Unit

The optical modulated signal is first fed to APD. The APD-PD pair of sensors converts the optical signal back into the electrical domain, which passes into the optical filter with a Bessel frequency transfer function centered at 28 GHz and a 2 dB filter bandwidth that successfully removes most of the noise. A coherent amplitude demodulator for quadrature components (I and Q) implements an analog demodulator of 64 levels, employing a 28 GHz carrier generator for quadrature components, being the component that regenerates an electrical baseband signal. The advanced digital signal processing (ADSP) unit, as shown in Fig. 3, compensates for digital domain degradation that assists in coherence detection of incoming transmission signal recovery.

Transmission channel bandwidth noise is added to the optically sampled signal, affecting the received RF signal. The voltages added to the modulators generate an additional DC shift. The higher shaping factor compensates this flatter phase delay and flatter group delay of the DC blocking third-order Bessel filter.

The output of the Bessel filter is sent through the fiber during the resampling process and the IQ compensation block is used to lower that. CD and non-linear compensation are included in this block, as are an adaptive equalizer and a down-sampling converter with carrier and frequency estimation [16].

After receiving IQ electrical signal channels from DSP, the decision component analyzes them, normalizes I and Q chan-
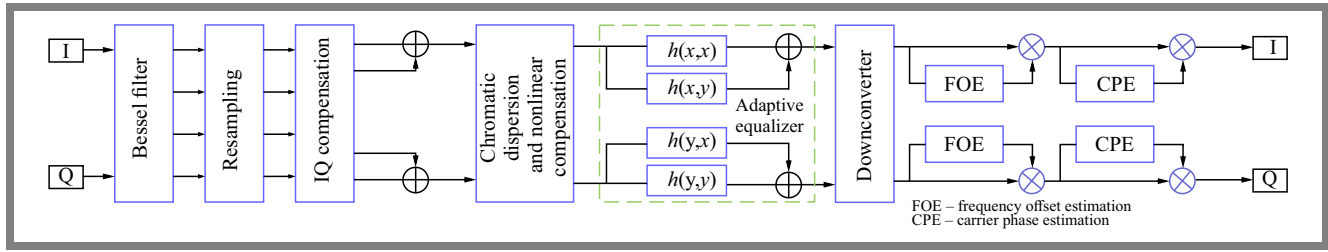
Fig. 3. Advanced DSP component block diagram; $h(x,y)$ is the tap weight of the signal's initial value, CPE is carrier phase estimation and FOE is frequency offset estimation.

nels' amplitudes to their corresponding 64 QAM levels and decides on each incoming symbol using the normalized threshold settings. The decision component performs the following functions (in order): DC blocking, decision, normalization, and EVM calculation.

The bit sequence is next recreated in the QAM sequence decoder using two concurrent input subsequences (I and Q quadrature carriers). This component generates a large bit sequence and transmits the bit sequence to the BER test set that refers it to the QAM pulse generator.

3.5. Link Performance

After sending a 64 QAM signal centered at 28 GHz via an optical fiber with a 140 km span, the proposed ARoF system's functionality was tested, and EVM was assessed. EVM is a simple metric used to quantify the combination of all signal impairments in a system. It calculates the difference between the "actual" value of the received signal and the "expected" complex value of a demodulated symbol. 3GPP has established that the EVM limit for 5G signals modulated using the 64 QAM modulation format is 8% and equals 3.5% for 256 QAM signals [20]. The root-mean-square values of EVM presented in this study are normalized to the average constellation power [21] as:

$$EVM\ [\%] = \sqrt{\frac{\frac{1}{M}\sum_{m=1}^{M}|S_m - S_{o,m}|^2}{\frac{1}{M}\sum_{m=1}^{M}|S_{o,m}|^2}}, \qquad (9)$$

where $S_{0,m}$ is the ideal normalized constellation point of the m-th symbol, S_m is the stream of the measured symbols' normalized m-th symbol, m defines how many unique symbols there are in the constellation, and S_m is the perfect normalized m-th symbol.

4. Simulation Results and Discussion

The effectiveness of the analog RoF system was evaluated using the parameter settings specified in Tab. 1. To ensure accuracy, the system underwent verification and EVM was calculated for a range of optical signal power levels, optical channel lengths, and MZM extinction ratios, during the design phase, using Optisystem software. The results were

analyzed to establish the system's performance under varying conditions.

A diagram of the RoF system is shown in Fig. 2. At the transmitter, the QAM signal is generated with a carrier frequency of 28 GHz and a data rate of 10 Gb/s. This QAM signal is split into two equal parts with a phase difference of 180°. The optical carrier developed from a CW wavelength of 1550 nm is modulated using parallel units MZM$_1$ and MZM$_2$. The MZM$_2$ output is further optically phase-shifted by 90° and the output of two MZMs is recombined using a power combiner to generate the optical modulated wave.

The optical spectrum and optical time domain waveform after the combiner are shown in Fig. 4.

Finally, such an optically modulated signal is transmitted over a 140 km SMF and 28 km DCF to compensate for the dispersion that affected the system's performance. The electric signal is recovered by an APD photodiode at the BS, as illustrated in Fig. 5. Later, this signal is filtered by a bandpass Bessel filter with a 28 GHz center frequency and 2 GHz bandwidth. The amplitude-coherent demodulator recreates the QAM data at a carrier frequency of 28 GHz. However, this signal is impacted by electro-optical conversion (E/O) loss and noise, non-linearity of the optical fibers, and channel phase noise. ADSP processes the baseband signal

Tab. 1. Simulation parameters.

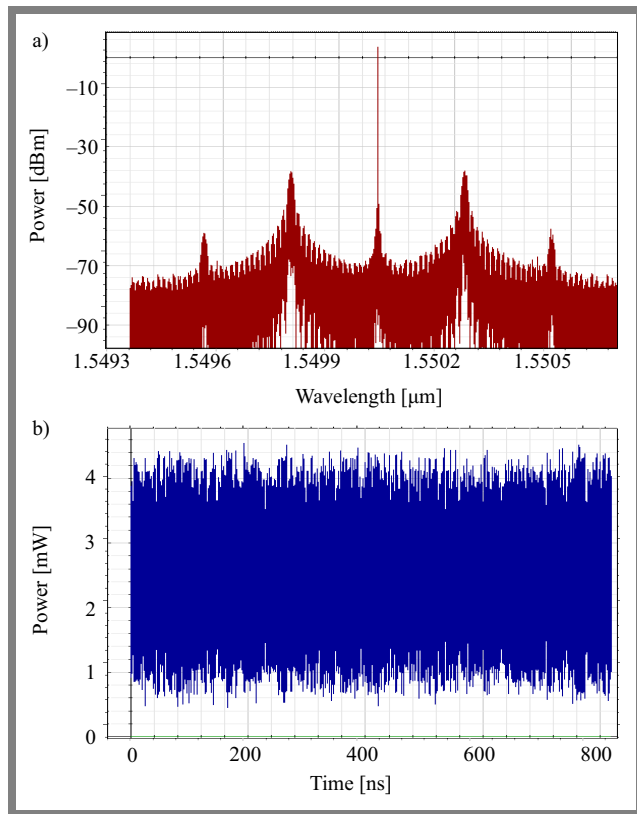| Parameter	Value
Bitrate	10 Gbit/s
Samples per bit	16
Modulation	64 QAM
Carrier frequency	28 GHz
Laser wavelength	1550 nm
CW linewidth	0.1 MHz
CW laser power	10 dBm
MZM extinction ratio	10 dB
APD-PD gain	5
Fiber attenuation	0.2 dB/km
Fiber dispersion	17 ps/nm/km
DCF attenuation	0.5 dB/km
DCF dispersion	−85 ps/nm/km

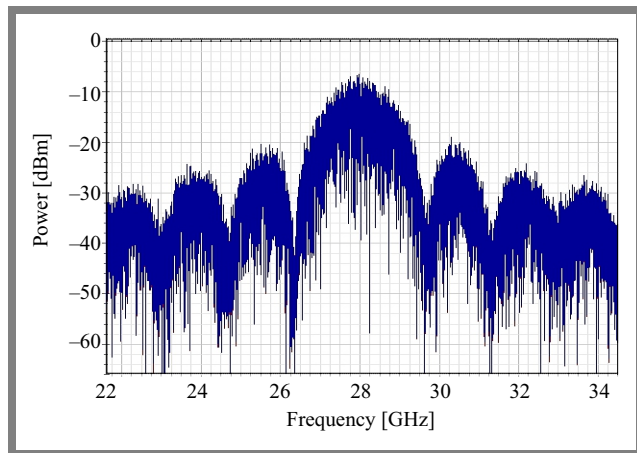**Fig. 4.** Waveforms of: a) optical spectrum after combiner and b) optical time signal.

Fig. 5. Recovered electric signal spectrum.

using a variety of approaches, beginning with preprocessing, and concluding with signal recovery.

Figure 6 shows the received baseband 64 QAM signal before ADSP and the corresponding constellation diagram after transmitting it through 140 km of fiber. The optical and RF channel parameters are bad due to the phase misfit of the symbol path. Hence, an ADSP block is utilized to improve them.

Figure 7 shows the 64 QAM signal and the corresponding constellation diagram next to the ADSP block. The demodulated signal is then processed in the decision component, where EVM of the received QAM symbol can be determined. The EVM for the proposed method is 7.709% after the signal
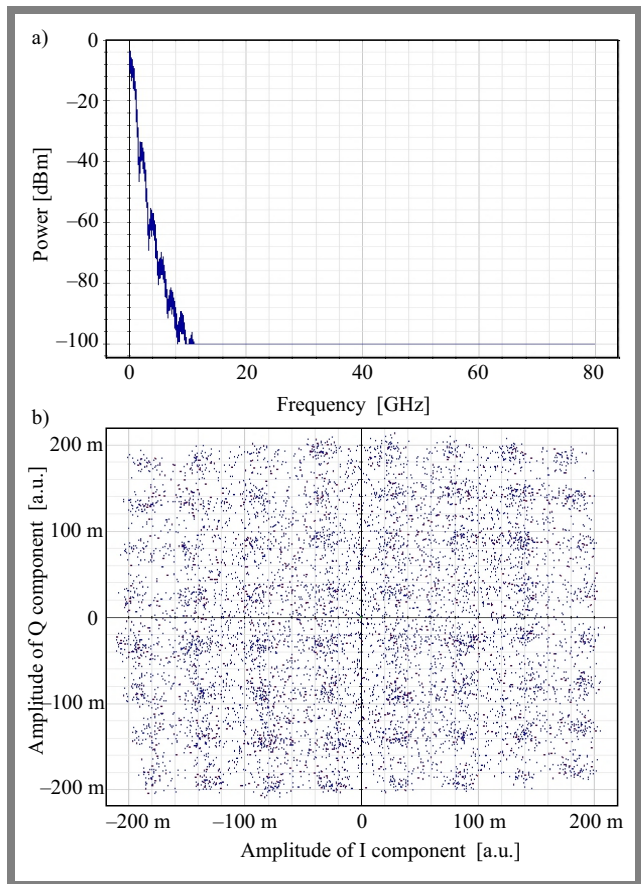

Fig. 6. 64 QAM signal before the ADSP a) and constellation diagram before ADSP b) (a.u. – arbitrary units).

passes through a 140 km fiber channel. The constellation diagrams show a significant improvement in the symbol path after passing through the ADSP block, which includes chromatic dispersion compensation, IQ imbalance compensation, channel equalization, FOE, and CPE signal recovery. The post-received signal is transformed into a digital bitstream after passing through the 64 QAM demodulator with a 6 bits/symbol set.

To test the system for different power levels, CW optical power was varied and EVM was evaluated for each case, as shown in Fig. 8a containing EVM vs. CW laser power plots for a 140 km SMF and a 28 km DCF. From the figure, one may observe a decrease in linearity of EVM values as the laser power increases. Laser power of 10 dBm is the optimal value at the EVM 3GPP limit for the 64 QAM signal.

The EVM value decreases even further with higher CW power levels, finally reaching 20 dBm. After this point, the EVM value will elevate rapidly.

The relation between the EVM value and different fiber lengths is plotted in Fig. 8b, showing the EVM result after the optical link length changes from 12 to 180 km. In this work, we used the loop control component that is available in the Optisystem program to simulate different optical channel lengths. Each loop consists of 10 km SMF and 2 km DCF to compensate for SMF's chromatic dispersion effect. In this case, EVM is 7.709% after passing through a 140 km SMF

Tab. 2. Comparison with recent research projects.

Reference	Modulation	Fiber length [km]	EVM [%]	Carrier frequency [GHz]	Optical modulation type	Data rate [Gbps]
Proposed	64 QAM	140	7.709	28	External	10
[10]	64 QAM	2	8.02	28	Direct	10
[12]	64 QAM	50	6.87	24	Direct	6
[12]	32 QAM	100	10.80	25	Direct	5
[22]	64 QAM	10	6.46	24	External	4.68
[23]	64 QAM	20	7.00	5	External	2.5
[24]	64 QAM	2	5.40	26	External	1.3
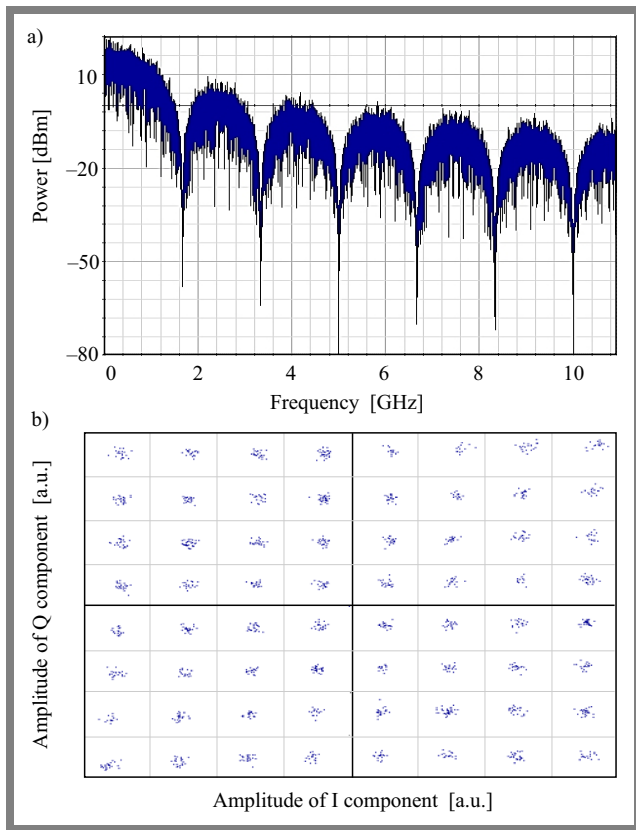
Fig. 7. 64 QAM signal after ADSP block a) and constellation diagram after ADSP block b).

Fig. 8. EVM vs. CW laser optical power curve a) and EVM vs. number of loops (fiber length) b).

Fig. 9. EVM vs. MZM excitation ratio.

and 28 km DCF, meaning that it remains below the maximum 3GPP limit of 8%.

A plot showing the EVM value versus MZM excitation ratio (ER) is shown in Fig. 9. It proves that a MZM result of 10 dB ER is optimal. Higher values cause a decrease in EVM.

It is clear from Figs. 8 and 9 that EVM values remain below the 3GPP limit, thus allowing to transmit C-band 64 QAM signals over long optical-fiber-link-based ARoF systems – a solution that improves simplicity and lowers cost due to lower transmitted power requirements. Hence, communication links are capable of delivering high-quality data complying with the 3GPP-EVM specification for 64 QAM signals.
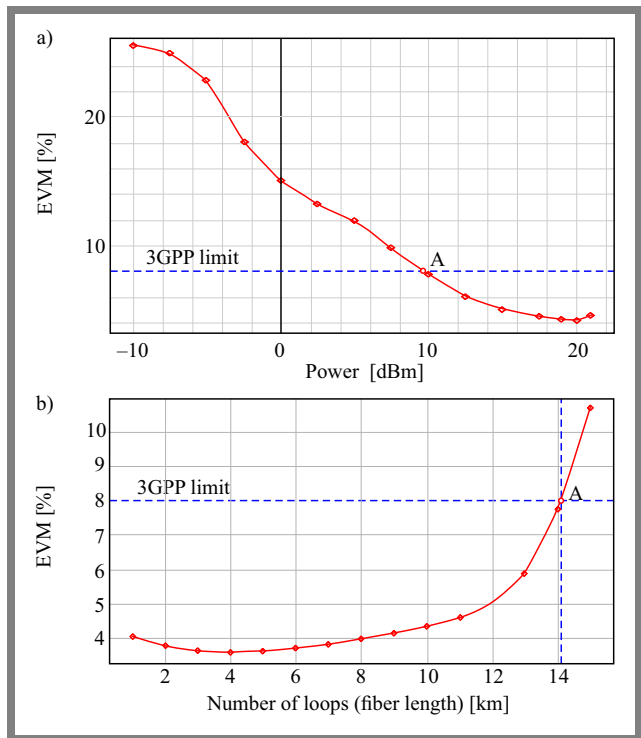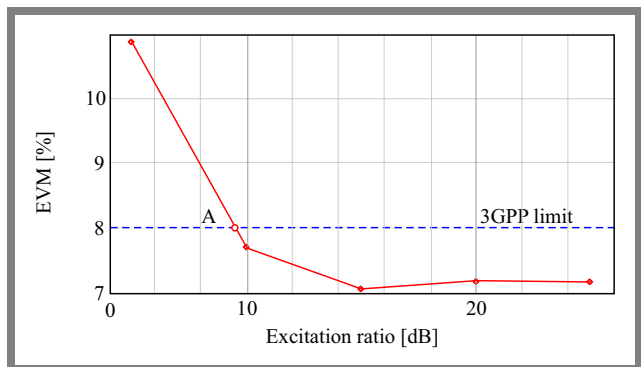
To validate the effectiveness of the proposed approach, an alternative design was evaluated as well, as shown in Fig. 10a. Unlike the parallel MZMs used in the previous design, this
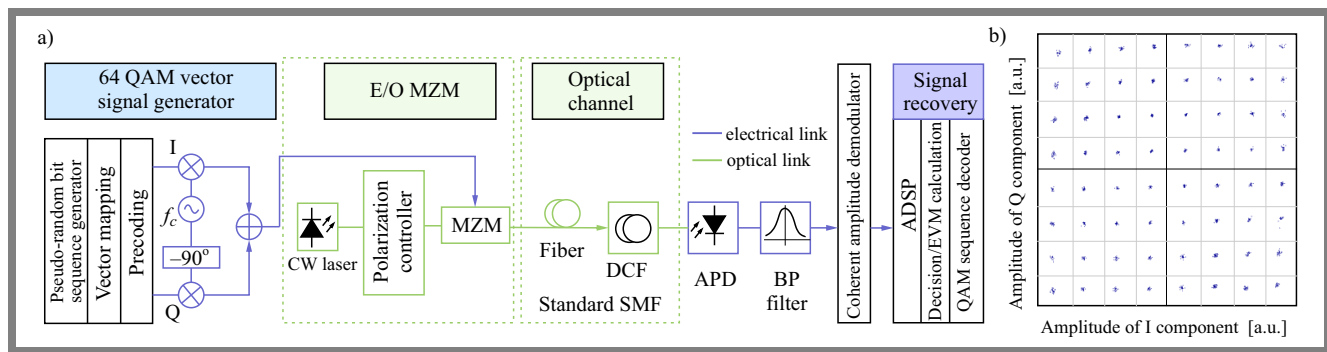
Fig. 10. Single MZM circuit design a) and corresponding constellation diagram after ADSP block b).

design uses only one MZM block to convert electrical signals into their optical counterparts. The results showed that the signal was received successfully after being transmitted over a 68 km SMF and a 17 km DCF. In this case, EVM equaled 5.88%. The constellation diagram of the received signal after ADSP is presented in Fig. 10b.

In addition, the proposed method was finally tested using an erbium-doped fiber amplifier (EDFA) instead of using the DCF. The experiment shows that such a setup is capable of transmitting 64 QAM signal over a 28 km-long optical fiber and a 5 m EDFA with 6.9% EVM, which indicates the advantages of using the optical amplifier and DCF.

Table 2 presents the outcomes of an analysis comparing the proposed technique and previous research projects across various data rates, considering the same modulation type and different carrier frequencies. One may see that at a high data rate of 10 Gbps (as in 10), direct modulation falls short, achieving a maximum transmitted distance of 2 km. In contrary, at a 6 Gbps bitrate (as in [12]), the fiber length can be extended up to 50 km at the carrier frequency of 24 GHz. Furthermore, the introduction of an external modulator with a data rate of 4.68 Gbps and the same 24 GHz carrier frequency allows to achieve a fiber distance of 10 km, as demonstrated in [22].

The proposed system, relying on ADSP and DCF techniques, supports longer distances with a high data rate, maintaining EVM within its standard limits. So, the proposed method offers satisfactory performance of RoF systems relying on long haul optical communication systems.

5. Conclusion

This study investigates a high data rate mmWave ARoF transmission relying on externally modulated parallel MZMs and evaluates its performance based on EVM. A 64 QAM signal in the frequency band of 28 GHz at 10 Gbps is successfully transmitted over a 140 km-long fiber with an EVM of 7.709%.

Different case studies show that when using EDFA instead of DCF, the transmission distance decreases to 28 km with 6.9% EVM. The experiment shows also that when using one MZM instead of two parallel MZMs, the signal was successfully received over a distance of 68 km, with an EVM of 5.88%,

which proves that the approach using parallel MZMs has certain advantages.

The proposed design combines adaptive deployment, low-latency strategies, advanced signal processing, and optical innovations to create a robust 5G network architecture. It not only overcomes existing challenges, but also paves the way for efficient and reliable communication in the 5G era. Furthermore, the proposed method appears to be superior to solutions described in the literature, and is suitable for long-haul next generation communications.

References

[1] P. Meena, M.B. Pal, P.K. Jain, and R. Pamula, "6G Communication Networks: Introduction, Vision, Challenges, and Future Directions", *Wireless Personal Communications*, vol. 125, no. 2, pp. 1097–1123, 2022 (https://doi.org/10.1007/s11277-022-09590-5).

[2] B. Kaur and N. Sharma, "Radio Over Fiber (RoF) for Future Generation Networks", in: *Broadband Connectivity in 5G and Beyond*, pp. 161–184, 2022 (https://doi.org/10.1007/978-3-031-06686-9_9).

[3] D.F. Paredes-Páliz *et al.*, "Radio Over Fiber: An Alternative Broadband Network Technology for IoT", *Electronics*, vol. 9, no. 11, pp. 1–8, 2020 (https://doi.org/10.3390/electronics9111785).

[4] B. Bae *et al.*, "24-40 GHz Dual-band Highly Linear CMOS Upconversion Mixer for mmWave 5G NR FR2 Cellular Applications", *IEEE Microwave and Wireless Components Letters*, vol. 32, no. 8, pp. 999–1002, 2022 (https://doi.org/10.1109/LMWC.2022.3161092).

[5] X. Zeng *et al.*, "Constellation Independent Look-up Table Enabled Digital Predistortion for Digital-Analog Radio-over-fiber System", *Optical Fiber Communications Conference and Exhibition (OFC)*, San Diego, USA, 2023 (https://doi.org/10.1364/OFC.2023.Tu2J.5).

[6] S.A.S. Saffar, "A Review on Radio Over Fiber Systems for Long Distance Communication", *Academic Journal of Nawroz University*, vol. 11, no. 3, 2022 (https://doi.org/10.25007/ajnu.v11n3a1363).

[7] K.A. Abdulrahman and J.J. Hamad Ameen, "Interference Effect Evaluation with Radio Over Fiber in 5G Mobile System", *Iraqi Journal of Computers, Communications, Control, and Systems Engineering*, vol. 23, no. 1, pp. 84–94, 2023 (https://doi.org/10.33103/uot.ijccce.23.1.7).

[8] H. Hamadouche, B. Merabet, and M. Bouregaa, "Performance Analysis of WDM PON Systems Using PIN and APD Photodiodes", *International Journal of Computer Aided Engineering and Technology*, vol. 18, no. 1–3, pp. 1–18, 2023 (https://doi.org/10.1504/IJCAET.2023.127785).

[9] J. Bohata *et al.*, "Transmitters for Combined Radio Over a Fiber and Outdoor Millimeter-wave System at 25 GHz", *IEEE Photonics*

Journal, vol. 12, no. 3, 2020 (https://doi.org/10.1109/JPHOT.2020.2997976).

[10] J. Van Kerrebrouck *et al.*, "10 Gb/s Radio-over-fiber at 28 GHz Carrier Frequency Link Based on 1550 nm VCSEL Chirp Enhanced Intensity Modulation after 2 km Fiber", *2018 Optical Fiber Communications Conference and Exposition (OFC)*, San Diego, USA, 2018 (https://ieeexplore.ieee.org/document/8386021).

[11] J. Bohata *et al.*, "24–26 GHz Radio-over-fiber and Free-space Optics for Fifth-generation Systems", *Optics Letters*, vol. 43, no. 5, pp. 1035–1038, 2018 (https://doi.org/10.1364/OL.43.001035).

[12] R.K. Shiu *et al.*, "A Simplified Radio-over-fiber System for Over 100-km Long-reach n-QAM Transmission", *IEEE Photonics Journal*, vol. 12, no. 3, 2020 (https://doi.org/10.1109/JPHOT.2020.2993180).

[13] M. Vukomanović, M. Šprem, Z. Šipuš, and D. Babić, "10-MSymbols/s QAM-16 Externally-modulated Optical Link for Radio-over-fiber Applications", *2018 41st International Convention on Information and Communication Technology, Electronics and Microelectronics (MIPRO)*, Opatija, Croatia, 2018 (https://doi.org/10.23919/MIPRO.2018.8400021).

[14] B. Zhang, Y. Qu, and M. Chen, "Simulation and Performance Study of Quadrature Amplitude Modulation and Demodulation System", *IOP Conference Series: Materials Science and Engineering*, vol. 782, 2020 (https://doi.org/10.1088/1757-899X/782/4/042048).

[15] T.N. Bakhvalova, D.A. Fofanov, A.V Alyoshin, and M.E. Belkin, "Fiber Distribution Networks with Direct and External Modulation of Digital QAM-signals", *2019 42nd International Conference on Telecommunications and Signal Processing (TSP)*, Budapest, Hungary, 2019 (https://doi.org/10.1109/TSP.2019.8768838).

[16] D. Chack and S.N. Thool, "High Capacity 64-Quadrature Amplitude Modulation Based Optical Coherent Transceiver for 60 GHz Radio Over Fiber System", 2023 (https://doi.org/10.21203/rs.3.rs-586845/v1).

[17] R. Atta, N. Sarkar, B. Dutta, and A.S. Patra, "A 40-Gbps Fiber-FSO Convergent Transmission System Employing OFCL-based WDM and External Modulation Technique", *Results in Optics*, vol. 11, art. no. 100421, 2023 (https://doi.org/10.1016/J.RIO.2023.100421).

[18] H. Li *et al.*, "Low Power All-digital Radio-over-fiber Transmission for 28-GHz Band Using Parallel Electro-absorption Modulators", *Optical Fiber Communication Conference 2020*, San Diego, USA, 2020 (https://doi.org/10.1364/OFC.2020.M2F.6).

[19] S. Kheris and B. Bouabdallah, "Analysis Three Dispersion Compensation Techniques using DCF", *Journal of Optical Communications*, vol. 44, no. s1, pp. 1469–1474, 2023 (https://doi.org/10.1515/joc-2020-0220).

[20] Y. Li and M. El-Hajjar, "Intelligent Analog Radio Over Fiber Aided C-RAN for Mitigating Nonlinearity and Improving Robustness", *IEEE Symposium on Computers and Communications (ISCC)*, Rhodes, Greece, 2022 (https://doi.org/10.1109/ISCC55528.2022.9912819).

[21] M.U. Hadi, H. Jung, P.A. Traverso, and G. Tartarini, "Experimental Evaluation of Real-time Sigma-delta Radio Over Fiber System for Fronthaul Applications", *International Journal of Microwave and Wireless Technologies*, vol. 13, no. 8, pp. 756–765, 2021 (https://doi.org/10.1017/S1759078720001282).

[22] H. Li *et al.*, "Real-time 100-GS/s Sigma-delta Modulator for All-digital Radio-over-fiber Transmission", *Journal of Lightwave Technology*, vol. 38, no. 2, pp. 386–393, 2020 (https://doi.org/10.1109/JLT.2019.2931549).

[23] M.R.N. Babir and P.K. Choudhury, "On the Performance of High Order QAM Signals for Analog and Digital Radio Over Fiber Systems", *2017 4th International Conference on Advances in Electrical Engineering (ICAEE)*, Dhaka, Bangladesh, 2017 (https://doi.org/10.1109/ICAEE.2017.8255385).

[24] K. Van Gasse *et al.*, "Silicon Photonics Radio-over-fiber Transmitter Using GeSi EAMs for Frequency Up-conversion", *IEEE Photonics Technology Letters*, vol. 31, no. 2, pp. 181–184, 2019 (https://doi.org/10.1109/LPT.2018.2889537).

———————

Hasan k. Al Deen, M.Sc.
College of Engineering, Electrical Engineering Department
https://orcid.org/0000-0003-0865-7472
E-mail: hasan.hasan.engh442@student.uobabylon.edu.iq
University of Babylon, Babylon, Iraq
https://www.uobabylon.edu.iq

Haider J. Abd, Ph.D.
Biomedical Engineering Department
https://orcid.org/0000-0002-5381-2446
E-mail: haider.jabber@uomus.edu.iq
University of Babylon, Babylon, Iraq
https://www.uobabylon.edu.iq
Al-Mustaqbal University, Hilla, Iraq
https://uomus.edu.iq/en/